International Journal of Antimicrobial Agents 66 (2025) 107596

Contents lists available at ScienceDirect

International Journal of Antimicrobial Agents

journal homepage: www.elsevier.com/locate/ijantimicag

Structural and functional features of *Klebsiella pneumoniae* capsular degradation by the phage depolymerase KP32gp38: implications for vaccination

Valeria Napolitano[a,†], Mario Privitera[a,†], Zuzanna Drulis-Kawa[b,c], Daniela Marasco[d], Silvia Fallarini[e], Rita Berisio[a], Flavia Squeglia[a,*]

[a] *Institute of Biostructures and Bioimaging, CNR, Napoli, Italy*
[b] *Department of Pathogen Biology and Immunology, University of Wrocław, Wrocław, Poland*
[c] *ESCMID Study Group for Non-Traditional Antibacterial Therapy (ESGNTA) member*
[d] *Department of Pharmacy, University of Naples Federico II, Napoli, Italy*
[e] *Department of Pharmaceutical Sciences, DSF, University of Piemonte Orientale, Novara, Italy*

ARTICLE INFO

Article history:
Received 17 January 2025
Accepted 8 August 2025

Editor: Ruby Lin

Keywords:
Klebsiella pneumoniae
Phage depolymerase
Protein structure
CPS degradation
Immune response induction

ABSTRACT

Objective: *Klebsiella pneumoniae Przondovirus* KP32 presents a complex capsular degradation machinery comprised of two serotype-specific depolymerases, KP32gp38 and KP32gp37.
Methods: In this work, we performed capsular polysaccharide (CPS) degradation assays combined with mass spectrometry approaches to identify the reaction product of K21 serotype CPS degradation by KP32gp38. We determined the crystal structure of the KP32gp38 depolymerase in complex with the identified degradation product, a pyruvated pentasaccharide, called K21-pyr5.
Results: The structure showed that K21-pyr5 binds to the inter-chain catalytic site, allowing the identification of important residues for CPS recognition. Importantly, we observed that the production of K21-pyr5 through CPS degradation by KP32gp38 is able to induce the maturation and differentiation of monocyte-derived dendritic cells, which, in turn, induce lymphocyte proliferation and Th polarization. By employing a T7 phage of *Escherichia coli* analogy, we were able to provide insights into the portal assembly of the *Przondovirus* K32. Our modeling studies suggest that the KP32 portal, attached to its icosahedral capsid shell, carries 12 depolymerase molecules on a single virion, arranged in 6 branches; in each branch, KP32gp38 depolymerase adheres to KP32gp37, which is directly connected to the phage portal.
Conclusions: Overall, our results suggest that depolymerases act as anti-virulent agents, not only by depleting the bacteria of their CPS but also by producing immunostimulatory CPS degradation products. This indicates the use of CPS degradation products by depolymerases as potential antigens in *K. pneumoniae* vaccination strategies.

1. Introduction

The advent of multidrug-resistant bacteria has rapidly emerged on a global scale, spreading between countries faster than previously anticipated. Excessive and improper use of broad-spectrum antibiotics in health care settings is thought to be a major cause of this drug resistance [1]. More than 1 million people per year died from drug-resistant infections between 1990 and 2021, and this could increase to nearly 2 million by 2050 [2]. The World Health Organization released a list of six alarming nosocomial pathogens that urgently require the development of new antimicrobials [3]. This group of pathogens, formed by *Enterococcus faecium, Staphylococcus aureus, Klebsiella pneumoniae, Acinetobacter baumannii, Pseudomonas aeruginosa*, and *Enterobacter* spp., is denoted by the acronym 'ESKAPE' because of their ability to 'escape' the biocidal action of antibiotics classified as highly important for hu-

* Corresponding author.
E-mail address: flavia.squeglia@cnr.it (F. Squeglia).
† These authors contributed equally to this study.

https://doi.org/10.1016/j.ijantimicag.2025.107596

man medicine [4,5]. Among these, *K. pneumoniae* with its emerging carbapenem-resistant strains, has become one of the most important bacterial pathogens because of its exceptional ability to acquire exogenous resistance- and hypervirulence-encoding genetic elements [6]. *K. pneumoniae* is a Gram-negative, encapsulated, facultative anaerobic, nonmotile bacterium belonging to the *Enterobacteriaceae* family [7,8]. It causes human infections including pneumonia, urinary tract infections, bloodstream infections, and sepsis, especially in newborns and immunocompromised individuals [9]. The most critical virulence factor of this microbe is its thick capsule composed of capsular polysaccharide (CPS). Indeed, CPS, consisting of repeating subunits of three to six sugars, provides a physical barrier that protects the bacteria from phagocytosis by immune cells such as macrophages and neutrophils. In addition, it inhibits activation of the complement system, crucial for opsonization and lysis of pathogens [10]. In this scenario, the use of phage-derived proteins, such as depolymerases, is an interesting and attractive option for therapeutic antivirulence purposes because of their ability to hydrolyze bacterial CPS, thereby facilitating immune recognition and increasing bacterial susceptibility to antibiotics [11–13].

To date, various *K. pneumoniae*-targeting depolymerases have been identified that degrade diverse capsular serotypes: K1, K2, KL64 [14], K5 [15], and K63 [16]. In previous work, we demonstrated that the *K. pneumoniae Przondovirus* KP32 encodes two proteins with CPS-degrading activity, namely KP32gp37 and KP32gp38, which degrade the K3 and K21 capsular serotypes, respectively [17]. The K21 serotype has been detected in a range of clinical isolates, especially within hospital settings. Although this serotype is not considered one of the most prevalent or highly virulent serotypes, it is present in several multidrug-resistant strains [18]. We reported the crystal structure of KP32gp38 and found that the interaction between the two depolymerases is mediated by the N-terminal region of KP32gp38. Typical of tail spike proteins, all depolymerases are trimeric and their catalytic β-helix domain adopts a right-handed solenoid-like fold. It has also been shown that tail spike protein depolymerase catalytic sites can be located either in the cleft between the neighboring chains or intra-chain. In this latter case, we showed for the KP34gp57 depolymerase, acting on the K63 serotype, that monomeric and trimmed versions containing the sole catalytic domain can also be fully active [16]. Altogether, these data have revealed a variety of modes of action of depolymerases acting against the *K. pneumoniae* capsule, although a thorough study of their degradation mechanism and a structural depiction of their interactions with CPS substrate is still missing.

Here, we focused on the degradation reaction of CPS from *K. pneumoniae* 358 (K21 capsular serotype) by KP32gp38 derived from *Przondovirus* KP32 to identify degradation products and elucidate the mechanistic features of CPS degradation. Using mass spectrometry, we established that KP32gp38 depolymerase degrades CPS to a pyruvated pentasaccharide. Therefore, we solved the crystal structure of the complex of KP32gp38 with its CPS degradation product, thus identifying important interactions involved in substrate recognition. Importantly, we observed that the CPS degradation product was able to induce maturation and differentiation of monocyte-derived dendritic cells (MoDCs), which, in turn, induced lymphocyte proliferation and Th polarization. Finally, we propose a model of the architecture of the entire phage portal, which carries a complex branched system of depolymerases. These findings provide structural details of the CPS degradation machinery of *Przondovirus* KP32 and a solid foundation for considering depolymerases as potent antivirulent agents due to the twofold action of depleting bacteria of their CPS shield and releasing CPS fragments that activate the host immune response.

2. Materials and methods

2.1. Depolymerase KP32gp38 expression and purification

The gene sequence corresponding to the phage depolymerase KP32gp38 was previously cloned into the pEXP5-CT/TOPO expression vector (Invitrogen, Carlsbad, CA, USA) [17]. The recombinant vector was transformed into competent *E. coli* BL21(DE3) cells (Stratagene) for overproduction of the protein. The *E. coli* cells were grown at 37°C to an OD_{600} of ~0.6–0.7 in Luria Bertani medium containing 100 µg mL^{-1} ampicillin. A final concentration of 0.2 mM isopropyl β-D-1-thiogalactopyranoside was added to 1 L of culture, which was then incubated overnight at 20°C. Subsequently, the harvested cell pellet was resuspended in a lysis buffer containing 300 mM NaCl, 5%(v/v) glycerol, 10 mM imidazole, 20 mM Tris-HCl, pH 7.8, and a complete protease inhibitor cocktail (Roche Diagnostics, Mannheim, Germany), sonicated on ice and then centrifuged at 18,000 rpm for 30 min at 4°C.

Purification of the trimeric depolymerase was performed, as described in [17], in two steps: affinity chromatography using a HisTrap HP column (GE Healthcare Life Sciences, Boston, MA, USA), followed by size-exclusion chromatography using a Superdex 200 16/60 column (GE Healthcare Life Sciences, Boston, MA, USA). After the purification process, the protein was more than 95% pure according to SDS-PAGE and was concentrated using Amicon Ultra-4 spin columns (Merck Millipore, Darmstadt, Germany). The protein concentration was estimated using a NanoDrop 2000 Spectrophotometer (Thermo Fisher Scientific, MA, USA), with the concentered protein used for the subsequent degradation of bacterial exopolysaccharides of *K. pneumoniae*, crystallization experiments with its natural substrate, and immunological tests.

2.2. Extraction of bacterial exopolysaccharides from K. pneumoniae K21 type

Extraction and purification of exopolysaccharides from *K. pneumoniae* 358 K21 type was carried out according to the protocol described previously [17]. A total of 20 mL of each overnight *K. pneumoniae* culture in tryptic soy broth (bioMerieux, Marcy l'Etoile, France) was added to a broad-bottomed flask containing 200 mL tryptic soy broth (to provide a large surface for biofilm formation), with the biofilm cultivated for 5 days at 37°C under static conditions. After biofilm development, 1200 µL formaldehyde was added and the mixture was incubated at room temperature with shaking for 1 h to prevent cell lysis. The addition of 80 mL of 1 M NaOH, followed by a 3 h-long incubation with shaking, resulted in exopolysaccharide extraction. The supernatant containing exopolysaccharides was separated by centrifugation (16,800 × *g*, 1 h, 4°C) and dialyzed against distilled water (12–14 kDa molecular weight cut-off membrane, SERVA Electrophoresis GmbH, Heidelberg, Germany) overnight. The addition of trichloroacetic acid (SERVA Electrophoresis Gmbh) to a final concentration of 20% and incubation on ice for 0.5 h was performed for protein and nucleic acid precipitation. Subsequently, 1.5 volumes of cold 96% ethanol (VWR, Radnor, PA, USA) was added to the supernatant, separated by centrifugation (16,800 × *g*, 1 h, 4°C), to precipitate exopolysaccharides from lipids during a 24 h-long incubation at −20°C. Exopolysaccharides were centrifuged (16,800 × *g*, 1 h, 4°C), the supernatant discarded, and the pellet resuspended in ultrapure water. The exopolysaccharide solution then was dialyzed against Milli-Q water (12–14 kDa molecular weight cut-off membrane, SERVA Electrophoresis GmbH) overnight followed by lyophilization. Lyophilized exopolysaccharides were then resuspended in ultrapure water to a desired concentration.

2.3. Digestion of capsular polysaccharide from Klebsiella K21 type by KP32gp38

The digestion procedure was carried out as reported earlier in [16]: 3.0 mg lyophilized surface polysaccharide from *Klebsiella* 358 K21 type was incubated with 600 µg pure KP32gp38. The reaction was performed at 37°C for 5 h in a 150 mM NaCl and 50 mM Tris-HCl buffer, pH 7.8. Digestion was stopped by adding trypsin and heating to 100°C for 10 min. The denatured protein was removed by centrifugation at 14,200 rpm and the digested products, present in the supernatant, were lyophilized for subsequent analyses by mass spectrometry and co-crystallization/soaking experiments. Quantification of the oligosaccharides was performed using the phenol-sulfuric acid colorimetric method [19]. Sample absorption was measured at 490 nm and compared to a calibration curve generated using known glucose concentrations.

2.4. Mass spectrometry analysis of digested products

CPS fragments were examined using tandem mass spectrometry (MS/MS). MS analysis was carried out on an LTQ XL mass spectrometry system (Thermo Fisher Scientific) with an ESI source in the positive-ion mode, mass range 200–2000 m/z. Mass calibration was carried out automatically by using selected multiply charged ions from a standard mixture (caffeine, Met-Arg-Phe-Ala peptide, Ultramark, Thermo Fisher Scientific). The general MS/MS conditions were as follows: spray voltage = 3.5 kV; vaporizer temperature = 350°C; sheath gas (nitrogen) = 10; auxiliary gas (nitrogen) flow = 2 arbitrary units; ion transfer capillary temperature = 350°C. Fragmentation was induced by a single ion with a collision energy of 35 eV, mass range 250–2000 m/z.

2.5. Crystallization of the KP32gp38 complex, data collection, and refinement

Purified KP32gp38 protein in 150 mM NaCl, 50 mM Tris/HCl, pH 7.8, and 5% (v/v) glycerol was concentrated to 8 mg/mL, with the natural substrate, previously dissolved in the same buffer, added at 10 mM to the protein solution for co-crystallization experiments. Crystallization trials were conducted at 20°C using the hanging drop vapor-diffusion method as described previously, with crystals obtained after 1–2 days. The reservoir solution contained 0.2 M ammonium citrate tribasic pH 7.0 and 20% w/v polyethylene glycol 3350. Diffraction data were acquired at the ESRF facility in Grenoble, France, at a temperature of 100 K. The crystals were cryo-protected by quickly soaking them in a solution containing 0.03 M citric acid, 0.045 M BIS-TRIS propane (pH 6.4), 15% (wt/vol) polyethylene glycol 3350, and 25% (vol/vol) glycerol. Diffraction images were processed using HKL3000 [20].

The crystal structure of the enzyme complex with CPS degradation product (K21-pyr5) was determined upon starting from the isomorphous apo structure [17]. Crystallographic refinement was initially performed using 95% of the measured data with the CCP4 program suite [20], while the remaining 5% was reserved for the R_{free} calculation. Refinement started with data up to 2.5 Å resolution and increased in successive rounds of refinement to the highest resolution. The bulk solvent was modeled according to Babinet's principle, as implemented in the Refmac program [20]. The final refinement round was performed with the inclusion of riding hydrogens. After refinement, the localization of the CPS degradation product K21-pyr5 was determined by computing difference density maps. The K21-pyr5 structure was generated using the program Coot [21], with the sugar moiety modeled in the electron density map using Coot and refined using Refmac [22].

2.6. Molecular modeling

The three-dimensional structure models of KP32gp37, its complex with KP32gp38, and the entire portal of the KP32 phage were obtained using the most recently released AlphaFold3.0 modeling server (https://www.alphafoldserver.com), which generated five ranked models [23]. Model confidence was evaluated based on the predicted local distance difference test, a per-residue measure of model confidence. The predicted local distance difference test is scaled between 0 and 100, with higher scores reflecting greater confidence in the structural model.

2.7. Peripheral blood mononuclear cell isolation and immature MoDC generation

Peripheral blood mononuclear cells (PBMCs) were isolated by density gradients using Lymphoprep (Incyte, Morges, Switzerland), as previously described in [24,25]. Isolated PBMCs were resuspended in RPMI completed with 10% FBS (Incyte, Morges, Switzerland), 2 mM glutamine, 100 µg/mL kanamycin, 1 mM sodium pyruvate, 1% non-essential amino acid solution, and 0.01 mM β-mercaptoethanol. To obtain immature MoDCs, 2.5×10^5 PBMCs/well were plated in a 12 Molecular Weight (MW) and allowed to adhere for 1 h. Nonadherent cells were removed by gently washing with PBS and the remaining adherent monocytes were cultured in complete RPMI. Immature MoDCs were generated by culturing monocytes in the presence of 20 ng/mL GM-CSF and IL-4 for 5 days. When indicated, monocytes were isolated by negative selection for $CD14^+$ cells using a magnetic cell separation system (Miltenyi Biotec, Woking, UK). The isolated monocyte $CD14^+$ population demonstrated >90% purity, as determined by flow cytometry. Isolated monocytes were plated at 3×10^5 cells/well and differentiated as described above.

2.8. DC treatment

To assess the effect of compounds on immature MoDCs differentiation, immature MoDCswere treated with 1 and 10 µM of K21-pyr5 or 10 ng/mL of LPS (Sigma-Aldrich) as a positive control for 48 h. Prior to the assay the LPS concentration was measured in all samples using a commercial LAL assay (Pierce Chromogenic Endotoxin Quant Kit, Thermo Fisher Scientific), to exclude possible contaminations. After incubation, cell culture media were harvested, filtered by 0.2 µm filter, and stored at −80°C for further evaluation. DCs were harvested and labeled with fluorescent anti-human CD14, CD80, CD86, CD83, CD40, CD11c, and HLA-DR, and DC maturation was analyzed by flow cytometry.

2.9. Cytokine evaluation

The level of IL-12 and TNF-α released by treated DCs was evaluated using an ELISA kit (Biolegend, San Diego, CA, USA) according to the manufacturer's instructions. The IL-12 and TNF-α concentrations within the samples were determined by extrapolation from specific reference standard curves.

2.10. Allogenic T-cell proliferation

MoDCs were treated with 10 µM K21-pyr5 or 10 ng/mL LPS for 48 h, harvested, washed with PBS, and plated with allogenic nonadherent CFSE-stained PBMCs (1:10 DC/PBMC ratio). After 7 days of co-culture, cells were harvested, washed, and the CFSE dilution was analyzed by fluorescence-activated cell sorting.

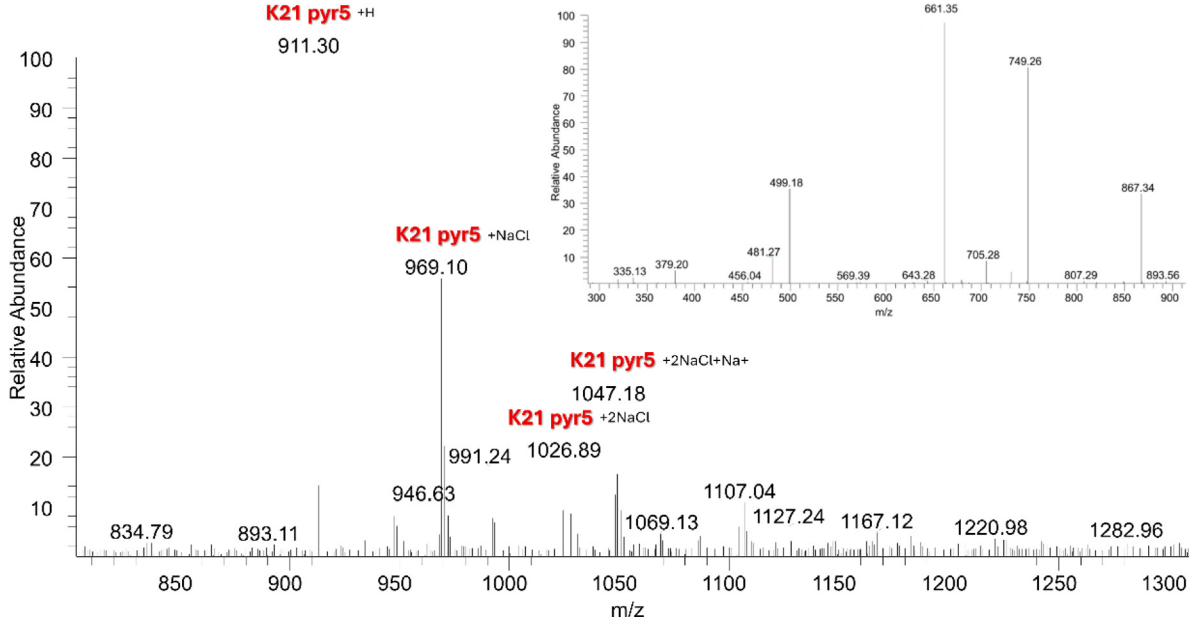

Fig. 1. Electrospray ionization-mass spectrometry spectrum of the digestion sample deriving from the CPS-KP32gp38 reaction mix, from which proteins were removed. Inset tandem mass spectrometry fragmentation of the peak at 911.3 m/z

2.11. T-cell polarization assay

MoDCs were treated with 10 µM K21-pyr5 or 10 ng/mL LPS for 48 h, harvested, washed with PBS, and plated with allogenic nonadherent PBMCs (1:10 DC/PBMC ratio). After 4 days of co-culture supernatants were harvested and IL-4 or IFN-γ levels were evaluated by ELISA assay.

2.12. Statistical analysis

Statistical analysis was performed using a two-way ANOVA using multiple comparisons. Results were considered significant when $p \leq 0.05$.

3. Results

3.1. KP32gp38 degrades CPS to a pyruvated pentasaccharide

We extracted and purified the CPS from *K. pneumoniae* 358 K21 type, whose structure was already described in [26]. Then, we employed electrospray ionization-mass spectrometry to identify the product of CPS digestion by KP32gp38. The MS spectrum (Fig. 1), exhibited a main peak at 911 m/z. On the basis of a reference study [26], this peak was assigned to an oligosaccharide containing 2 mannose, 2 galactose, 1 glucuronic, and 1 pyruvic acid moiety. The spectrum also presented ions deriving from monosodiate species and NaCl adducts due to the presence of NaCl at a high concentration (150 mM) in the digestion buffer. Tandem mass spectrometry fragmentation of the peak at 911 m/z (inset of Fig. 1) confirmed the monosaccharide identities. The main degradation product of the KP32gp38 enzymatic reaction, the pyruvated pentasaccharide, was denominated as K21-pyr5.

3.2. Crystal structure of KP32gp38 in complex with CPS reaction product

The CPS depolymerase KP32gp38 is a large enzyme with a trimeric organization consisting of 578 amino acid residues per chain and a MW, as a trimer, of ~200 kDa. We previously determined the crystal structure of KP32gp38 using anomalous dispersion techniques [17]. Well-diffracting crystals of the KP32gp38 complex with its CPS degradation product K21-pyr5 were successfully obtained using polyethylene glycol 3350 solutions as precipitants. Data at 1.8 Å resolution were recorded at ESRF in Grenoble. The structure, which contained one protein chain in its asymmetric unit, was refined against that of the apoenzyme [17] and included 548 amino acid residues and 660 water molecules. The N-terminal 30 residues could not be modeled in the electron density maps. The refinement of the structure including K21-pyr5 led to final R and R_{free} values of 18.8% and 23.5%, respectively (Table 1). Biological assembly of the KP32gp38 structure was generated through crystallographic symmetry using PISA [17,27], and analysis of the difference electron density maps clearly shows the localization of K21-pyr5 at the interface between two adjacent chains (Fig. 2). K21-pyr5 is embedded in a deep cleft (Fig. 3A) where its Gal moiety forms hydrogen bonding interactions with the Asp241 side chain, whereas the first Man moiety forms hydrogen bonding interactions with Tyr147 and Arg179 of the adjacent chain (Fig. 3B).

Table 1
Data collection and refinement statistics.

A. Data collection	Remote
Space group	$P3_2$
Unit-cell parameters: a, b, c (Å); β (°)	70.5, 70.5, 205.6; 120.00
Resolution range (Å)	60.0-1.8
Total reflections (n)	53170
Multiplicity	5.7
Completeness (%)	99.6 (99.8)
†R_{merge}	0.82 (0.44)
Average I/σ(I)	9.0
B. Refinement	
†R_{work}/R_{free} (%)	18.8, 23.5
Residues (n)	548
Waters (n)	660
R.m.s. deviations:	
Bond lengths (Å)	0.01
Bond angles (°)	1.6

Values in parentheses represent the highest resolution shell, 1.84–1.80 Å.
† $R_{merge} = \Sigma\ h\Sigma i\ |I(h,i)-<I(h)>|/\ \Sigma\ h\Sigma i\ I(h,i)$, where $I(h,i)$ is the intensity of the ith measurement of reflection h and $<I(h)>$ is the mean value of the intensity of reflection h.

A water molecule bridges the interaction of this Man moiety with the side chains of Glu170 and Ser146. Other hydrogen bonds with Arg179 and Arg180 were mediated by the Glc moiety. Furthermore, several hydrophobic interactions were established by K21-pyr5 with residues of both chains (Fig. 3B). In our previous study, a key catalytic role was proven for Asp241 and Glu170, as their mutation completely suppressed KP32gp38 enzymatic activity [17]. We consistently showed here that these two residues directly interact with K21-pyr5 through direct hydrogen bonding with its Gal moiety or water-mediated hydrogen bonding with its Man moiety (Fig. 3B). Glu239 and Asp229 appeared to be less important, but still relevant [17]. In the crystal structure of the KP32gp38-K21-pyr5 complex they did not make contact with K21-pyr5 (Fig. 2A) and were located in the empty carbohydrate subsite adjacent to the Gal moiety, in a position that likely makes contact with the adjacent sugar in the non-hydrolyzed CPS. Therefore, these two acidic residues are likely important for CPS recognition and stabilization of its conformation for optimal hydrolytic reaction, a step preceding catalysis. The crystal structure suggests a similar role for Arg179 and Arg180 in the CPS recognition event, as both residues interact with the Glc moiety of K21-pyr5 (Fig. 3B).

3.3. Structural clues on depolymerase branching: KP32gp38 attachment on KP32gp37

In a previous study, we predicted that diverse *Klebsiella* phage tailspikes, also known as Receptor-Binding Domains (RBPs), may assemble two or more tailspikes in the branching system via the T4gp10-like domain and conservative peptides [29]. In the case of KP32gp38, using isothermal titration calorimetry we proved that KP32gp38 strongly binds to the other RBP of *Klebsiella* phage KP32, KP32gp37, with a binding affinity in the low nanomolar range (K_D =21 ± 8 nM). We also proved that the structural domain of KP32gp38 for attachment to KP32gp37 is located at the N terminus, as a truncated variant of KP32gp38, lacking its N-terminal 29 amino acid fragment, was unable to bind KP32gp37 [17]. However, we were unable to provide a structural description of the interaction between the two depolymerases, given the poor sequence identity of KP32gp37 with proteins of known structure [17]. The revolution introduced by artificial intelligence has provided an opportunity to describe these important interactions. Indeed, modeling of KP32gp38 with AlphaFold3.0 [30] provided a structure that strongly resembled the experimental one, with a root mean square deviation between the two structures, computed on backbone atoms, of 3.2 Å (N). In the KP32gp38 crystal structures, the N-terminal 30 residues were not visible in the electron density maps. Consistently, the AlphaFold3.0 KP32gp38 model shows a helical region showing high flexibility, albeit with significant confidence (70 > plDDT > 50). Prompted by this observation, we also modeled the KP32gp37 structure using AlphaFold3.0 with high confidence (90 > plDDT > 70).

KP32gp37 presents a more complex and elongated structure compared with KP32gp38 (Fig. 4). An N-terminal module (residues 1–293) was formed by three coiled-coil regions, interrupted by trimers of lectin-like domains (Lectin1 and Lectin2 in Fig. 4). Structure alignment using DALI showed that the N-terminal 150 residues, embedding the N-terminal coiled-coil domain and Lectin1 domains (residues 1–146), share strong structural similarity with the adapter domain of tailspike gp17 belonging to the *E. coli* phage T7 (pdb 7ey9, DALI Z = 16.0; pdb 8dsp, DALI Z = 18.8) [31]. For this virus, the entire structure including the ejection proteins and in complex with their cell receptor LPS, was determined using cryo-EM [31]. A catalytic β-helix domain follows the N-terminal module and adopts the typical trimeric right-handed solenoid-like fold (Fig. 4) and this structure partially overlaps with the catalytic domain of KP32gp38, with a root mean square deviation of 3.4 Å.

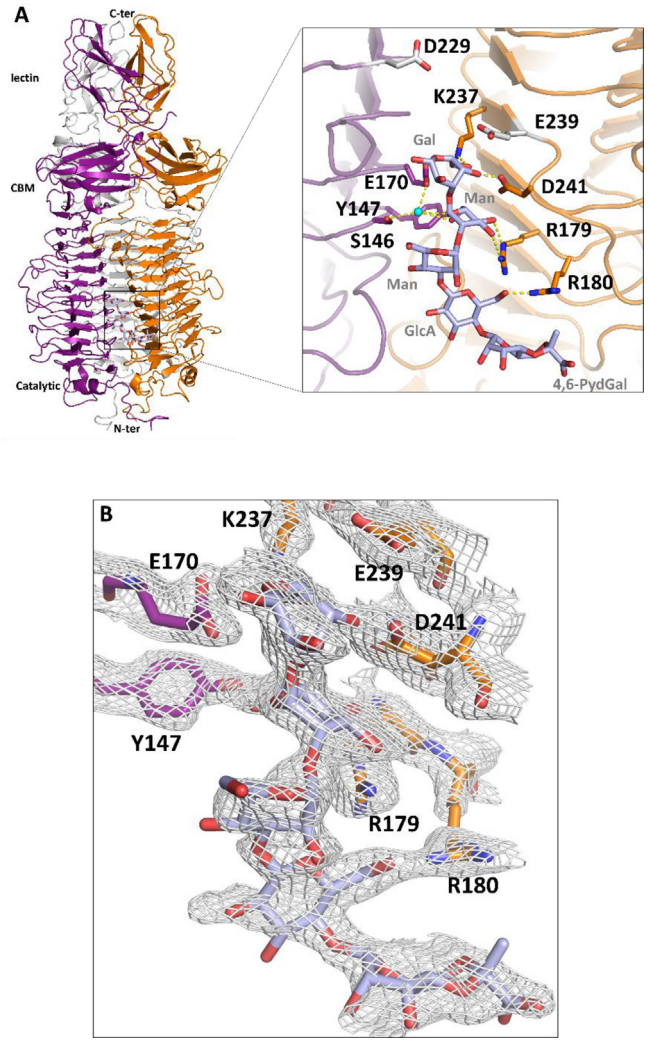

Fig. 2. (A) Schematic representation of the two chains of the KP32gp38 structure, showing the localization of K21-pyr5, reported in stick format, at their interface (PDB code: 9QRM). Inset image shows a magnification of the K21-pyr5 structure, with relevant residues drawn in stick representation. D229 and E239, which are not involved in ligand binding, are drawn in gray. A water molecule (cyan) bridges the K21-pyr5 interactions with Glu170 and Ser146. (B) (2Fo-Fc) electron density map, contoured at 2σ around the K21-pyr5 binding site.

Different from KP32gp38, KP32gp37 included an extra helical domain at its C-terminus (Fig. 4) that displayed strong structural resemblance (DALI Z = 12.8) to the intramolecular chaperone domain of the T5 phage L-shaped tail fiber, which underwent autocleavage at Ser 1264 [32]. Sequence alignment of the chaperone domains of the two structures shows an overall sequence identity of 27%, albeit with full conservation of the cleavage site (771-DSR-773 in KP32gp37), thus also suggesting auto-cleavage in KP32gp37. Indeed, auto-cleavage is considered a common feature among endosialidases and other tailspikes and tail fibers, as it traps the mature trimer into a more kinetically stable conformation [33,34].

Using AlphaFold3.0, we also modeled the structure of the complex between the two depolymerases (Fig. 4B). In this structure, the N-terminal helices of KP32gp38 acted as a hook through hydrogen bonding and hydrophobic interactions involving all three chains, either with residues of two lectin2 domains (e.g., hydrogen bonds with Arg224, His261, and Val227) or with residues of the third coiled-coil region (e.g., with Arg275; Supplementary Fig. S2). This binding fashion rendered KP32gp37 dissymmetric and allowed branching of the two depolymerases on the phage [29]. The

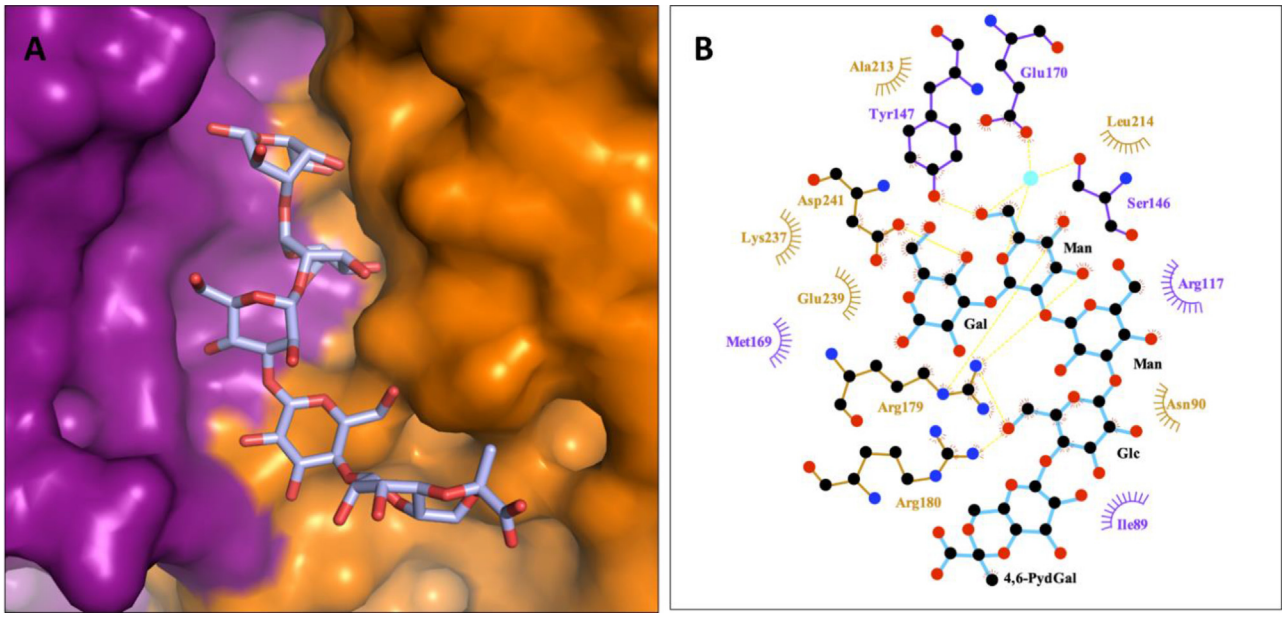

Fig. 3. (A) Stick representation of K21-pyr5, embedded in its inter-chain cleft of KP32gp38, drawn in surface representation. (B) Interactions of K21-pyr5 with KP32gp38, identified using LigPlot [28]. Chains A and B are drawn in purple and orange, respectively.

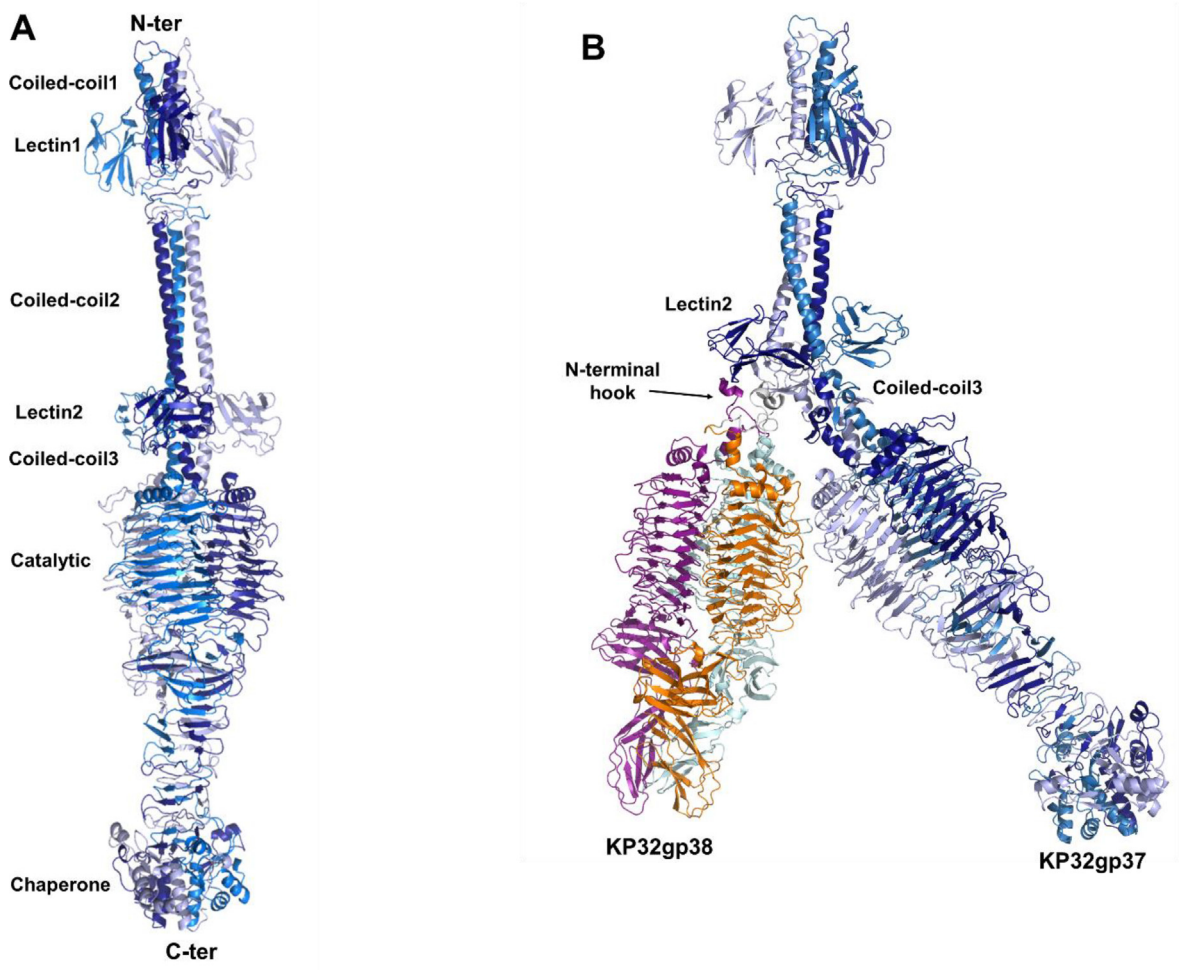

Fig. 4. Schematic representation of the complex between the KP32gp37 AlphaFold3.0 model (A) and KP32gp38 (B). KP32gp37 is represented by gradations of blue, whereas KP32gp38 is represented by orange/purple/gray.

Table 2
Structurally characterized depolymerases against *Klebsiella pneumoniae*, as reported in the literature.

Depolymerase	Oligomeric state	Catalytic site	Serotype specificity	Ref.	PDB code
KP32gp38	Trimeric	Inter-chain	K21	[17]	6TKU, 9QRM
KP34gp57	Trimeric	Intra-chain	K63	[16]	8BKE
Depo32	Trimeric	Inter-chain	K2	[40]	7VYV
K1 Lyase	Trimeric	Intra-chain	K1	[37]	7W1D
K64-ORF41	Trimeric	Intra-chain	K64	[38]	8 × 8M
DpK2	Trimeric	Inter-chain	K2	[39]	7LZJ

modeled binding mode was in full agreement with our previous binding studies [17], highlighting the key role of the N-terminal residues of KP32gp38 (e.g., Asp3, Asn6, and hydrophobic Leu2 and Phe5) in the binding of KP32gp37 [17].

3.4. CPS degradation product K21-pyr5 induces the maturation and differentiation of DCs

We evaluated whether the degradation product of the *K. pneumoniae* K21 CPS obtained by KP32gp38 activity (K21-pyr5), was able to induce DC maturation. To exclude any contamination by LPS, which is a well-known immune cell activator able to induce DC maturation, we first measured LPS concentration, which was below the detectable value (0.01 EU/mL). As an in vitro model, we used MoDCs, which are widely used in immunological studies. Immature DCs were used to evaluate the ability of K21-pyr5 to induce DC maturation. After 48 h of treatment at increasing concentrations (0.01–10 μg/mL) of K21-pyr5, we observed an increase in HLA- DR and costimulatory molecule expression (Fig. 5). In detail, we observed a concentration-dependent increase in the expression of CD40, CD80, CD83, and CD86. Of note, the increase obtained for CD80, CD86, and HLA-DR was larger than that induced by LPS (1 μg/mL) (Fig. 5A and B), and these data suggest that K21-pyr5 is able to induce immature DC maturation to a mature phenotype able to stimulate T-cell responses.

To better explore K21-pyr5–induced MoDC maturation, we evaluated the TNF-α and IL-12 levels released by DCs in a cell culture medium. During the maturation process, DCs acquired the ability to produce and release cytokines able to recruit and orchestrate immune cells toward a pro- or anti-inflammatory response. K21-pyr5 treatment induced the production and release of detectable levels of TNF-α and IL-12 when used at 1 and 10 μg/mL, suggesting the ability of K21-pyr5 to induce differentiation of MoDCs to a pro-inflammatory phenotype (Fig. 5C and D).

3.5. Lymphocyte proliferation and Th polarization induced by K21-pyr5-treated MoDCs

A mixed lymphocyte reaction was performed to evaluate the stimulatory ability of MoDCs treated with K21-pyr5. Treated MoDCs were cultured with allogenic lymphocytes for 7 days and proliferation was evaluated. As shown in Fig. 6A, K21-pyr5–treated MoDCs were able to induce higher lymphocyte proliferation when compared with a control. Indeed, a lower percentage of undivided cells was observed for K21-pyr5-treated MoDCs when compared with untreated MoDCs (Fig. 6A). Moreover, the number of lymphocyte cell divisions increased for K21-pyr5–treated MoDCs (Fig. 6B). In addition to the stimulation of T-cell proliferation, a key role of DCs was to shape the effector T-cell response through the polarization of naive CD4 T-cell differentiation. To investigate how K21-pyr5-treated MoDC affects polarization, the level of IFN-α and IL-4 was evaluated within the supernatant of the mixed lymphocyte reaction. K21-pyr5–treated MoDCs were able to induce a higher level of IFN-α when compared with control MoDCs (Fig. 6C). Instead, no significant increase in IL-4 level was observed, suggesting Th1 T-cell polarization (Fig. 6D). Overall, these results suggest that K21-pyr5–treated MoDCs stimulate T-cell proliferation and differentiation toward a pro-inflammatory phenotype.

4. Discussion

Phage-derived depolymerases are an attractive option to adjuvant the effect of antibiotics [11–13]. Given the relevance of the strong emergence of *K. pneumoniae* infections, especially from carbapenem-resistant *K. pneumoniae* strains, as well as the exceptional ability of this bacterium to evade the action of antibiotics and the immune system [6,35,36], *K. pneumoniae*-targeting depolymerases degrading diverse capsular serotypes have been identified as a promising therapeutic option [14,15]. Only recently have a limited number of depolymerase enzymes been structurally characterized [37–39]. All of them proved to be trimeric, with either inter-chain or intra-chain catalytic sites, although no information is hitherto available on the binding modes of their substrates (Table 2).

Phage KP32 belongs to group A of KP32 viruses (Przondoviruses) and has tailspikes attached to a short, noncontractile tail [29]. We previously demonstrated that phage KP32 encodes two proteins with different CPS-degrading activities, KP32gp37 and KP32gp38, which form a strong molecular complex and degrade K3 and K21 capsular serotypes, respectively [17]. In addition to KP32, other *K. pneumoniae* podoviruses possess two RBPs with different enzymatic specificity, including K5-2 and K5-4, whereas some phages possess a single RBP [41,42]. This suggests that RBP branching, through the complex formation of more depolymerases, is an efficient mechanism for extending the specificity toward different bacterial CPSs, although a molecular description of this branching has not been described. Similarly, it is not clear how these enzymes interact with their substrate.

Using mass spectrometry, we found that KP32gp38 depolymerase degrades CPS to a pyruvated pentasaccharide, K21-pyr5. The crystal structure of the complex of KP32gp38 with K21-pyr5 provides a structural explanation for the key catalytic role we previously observed for Asp241 and Glu170 [17], as these residues strongly interact with K21-pyr5. Analysis of these interactions also suggests the importance of arginine residues Arg179 and Arg180, which both interact with the Glc moiety of K21-pyr5, in CPS recognition and specificity. Importantly, we also observed that KP32gp38 degradation product K21-pyr5 induces the maturation and differentiation of MoDCs, which, in turn, promoted lymphocyte proliferation and Th polarization in a mixed lymphocyte reaction assay. These data suggest that phage depolymerases are also a powerful tool for preparing structurally defined oligosaccharides, enabling the development of glycoconjugate vaccines to combat infections caused by *K. pneumoniae*.

The use of artificial intelligence has allowed us a better understanding of the architecture of depolymerase-containing RBPs in the *Przondovirus* KP32. Indeed, AlphaFold3.0 modeling confirmed our experimental KP32gp38 structure [17] and allowed us to model the partnering KP32gp37 structure as well as the complex between the two depolymerases. Those in silicopredicted interactions were in full agreement with our previous data, showing a key role for the N-terminal residues of KP32gp38 in its binding to KP32gp37 [17]. KP32gp37 presents an articulated structure, carrying an ex-

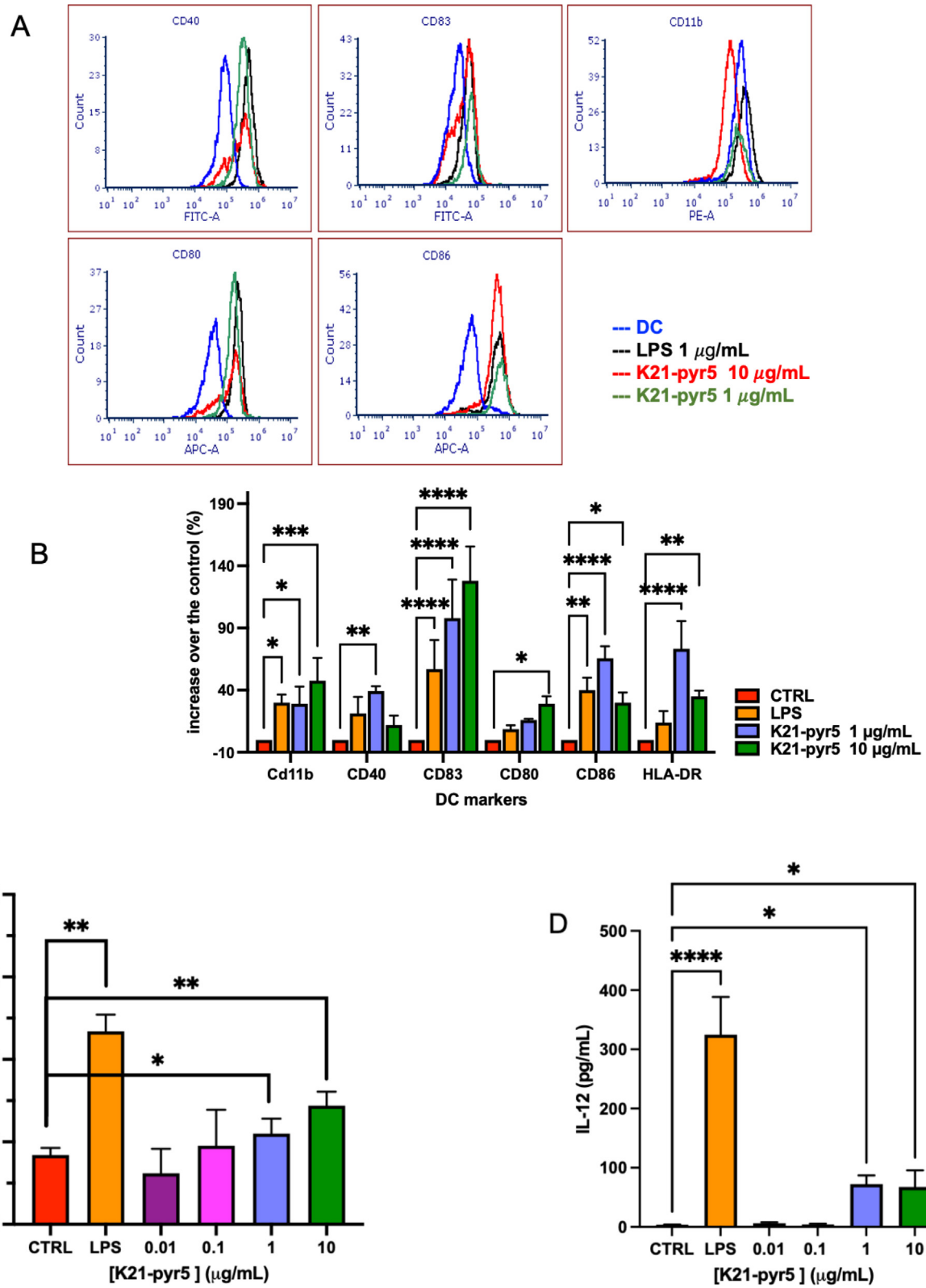

Fig. 5. Maturation of monocyte-derived dendritic cells (MoDCs) by K21-pyr5 and its effect on TNF-α and IL-12 release by MoDCs. Immature MoDCs were untreated/treated with increasing concentrations (1–10 μg/mL) of K21-pyr5 or lipopolysaccharide (LPS; 1 μg/mL) for 48 h. After incubation, MoDCs were harvested and stained with anti-human CD11b, CD40, CD80, CD83, CD86, and HLA-DR and analyzed by fluorescence-activated cell sorting. (A) Representative histograms of CD11b, CD40, CD80, CD83, CD86, and HLA-DR expression on immature MoDCs treated or untreated with KP32gp38 depolymerase capsular polysaccharide product or positive control (LPS). (B) Increase (% over the control) of CD11b, CD40, CD80, CD83, CD86, and HLA-DR on MoDC treated with K21-pyr5 or a positive control (LPS). Results are expressed as the mean ± standard error of the mean (SEM) of at least three independent experiments run in triplicate using MoDCs and T cells from different donors. $^{*}p \leq 0.05$; $^{**}p \leq 0.01$; $^{***}p \leq 0.0001$; $^{****}p \leq 0.00001$. (C) Effect of K21-pyr5 on TNF-α and (D) IL-12 release by MoDCs. Immature MoDCs were treated/not treated with increasing concentrations (1–10 μg/mL) of K21-pyr5 or LPS (1 μg/mL) for 48 h. After incubation, the MoDC supernatants were collected and stored at −80°C until analysis. TNF-α levels in the supernatant were evaluated by ELISA. The results are expressed as the mean ± SEM of at least three independent experiments run in triplicate using MoDCs and T cells from different donors. $^{*}p \leq 0.05$; $^{**}p \leq 0.01$.

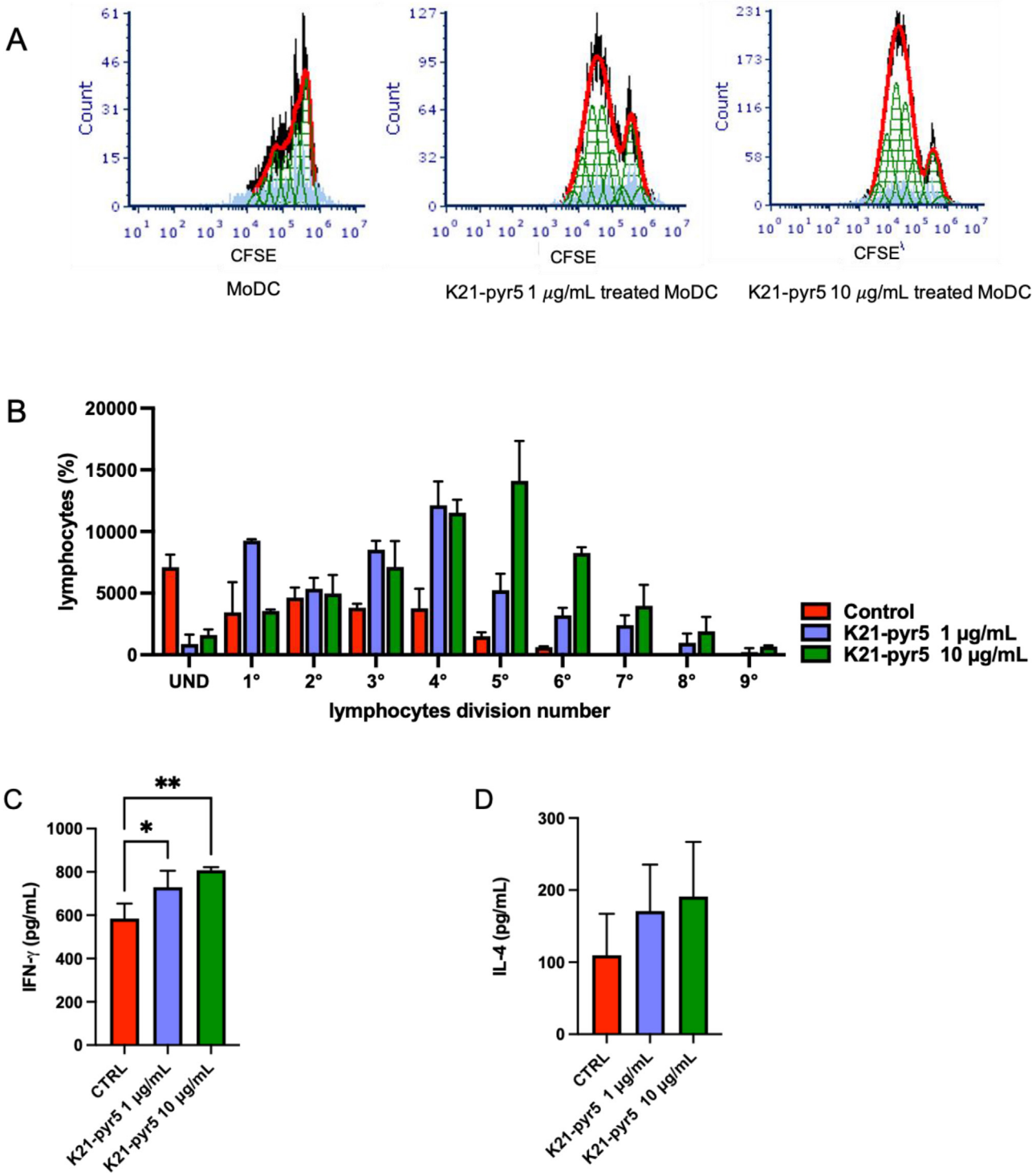

Fig. 6. Effect of K21-pyr5-treated monocyte-derived dendritic cells (MoDCs) on allogenic T-cell proliferation. Immature MoDCs treated/not treated with increasing concentrations (1–10 μg/mL) of K21-pyr5 for 48 h were cultured with Carboxy Fluorescein Succinimidyl Ester (CFSE)-stained allogenic T cells for 7 days. After incubation, the CFSE dilution was analyzed by fluorescence-activated cell sorting. (A) Representative histograms showing the proliferative responses in a mixed lymphocyte reaction (MLR) induced by MoDCs, MoDCs treated with 1 μg/mL K21-pyr5, and MoDCs treated with 10 μg/mL K21-pyr5. (B) Proliferation induced in MLRs by MoDCs, K21-pyr5 1 μg/mL-treated MoDCs, and K21-pyr5 10 μg/mL-treated MoDCs. Results are expressed as the mean ± standard error of the mean (SEM) of at least three independent experiments run in triplicate using MoDC and T cells from different donors. (C, D) Effect of K21-pyr5-treated MoDCs on Th polarization. Immature MoDCs treated/untreated with increasing concentrations (1–10 μg/mL) of K21-pyr5 for 48 h were cultured with allogenic T cells for 7 days. After incubation supernatants were collected and IFN-α (A) and IL-4 (B) levels were evaluated by ELISA. The results are expressed as mean ± SEM of at least three independent experiments run in triplicate using MoDCs and T cells from different donors. $^{*}p \leq 0.05$; $^{**}p \leq 0.01$.

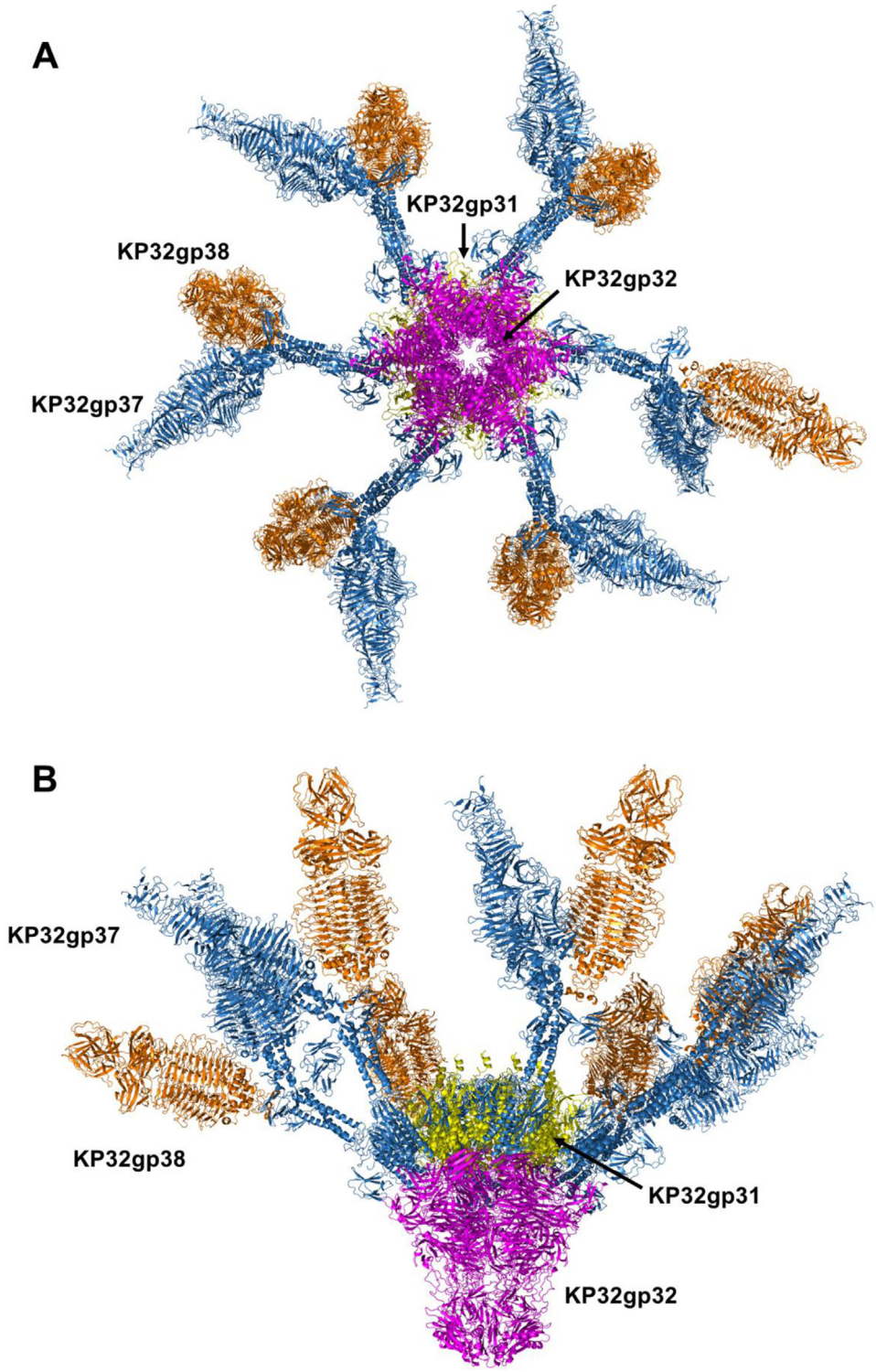

Fig. 7. Schematic representation of the proposed architecture of the phage KP32 tailed portal, based on its homologous portal from the *Escherichia coli* phage T7 (pdb code 7ey9 [31]). KP32gp31 and KPgp32, forming the KP32 portal, are drawn in yellow and magenta, respectively. Depolymerases KP32gp37 (deprived of its self-proteolyzed chaperone) and KP32gp38 are drawn in blue and orange, respectively. The bottom and side views are shown by (A) and (B), respectively.

tra chaperone-like domain at its C-terminus and an adapter domain at the N-terminal end. The C-terminal domain has a strong structural resemblance to the C-terminal domain of phage T5 L-shaped tail fiber and is absent in all other RBPs of group A KP32 viruses [29]. On the other hand, the large and complex structure of KP32gp37 likely explains the need for an intramolecular chaperone to allow its folding. Indeed, elongated trimeric beta-structured proteins have evolved different strategies to fold correctly, either folding endogenously when expressed in bacteria [43,44] or requiring specialized chaperone proteins [45–48]. Analogous to bacteriophage T5 L-shaped tail fibers [32], the C-terminal intramolecular chaperone of KP32gp37 is likely self-proteolyzed, given the full conservation of the proteolysis site within the two proteins.

The N-terminal 150 residues of KP32gp37 show strong structural similarity to the N-terminal region of the tail fiber gp17 from the mature *E. coli* podophage T7 (pdb 7ey9, DALI $Z = 16.0$; pdb 8dsp, DALI $Z = 18.8$; sequence identity 45%) [31]. Its portal was structurally described as being comprising a 12-fold assembly of protein gp11 and a sixfold nozzle assembly of protein gp12 [31]. In this structure, six subunits of the trimeric tail fiber gp17 decorate the portal [31]. Using a BlastP search, we found that proteins constituting the *E. coli* phage T7 present strong sequence identity with those of the phage KP32 (taxid 674082). Namely, gp11 of T7 was 62.2% identical to the KP32 tail tubular protein A (TTPA), YP_003347549.1, locus tag KP32gp31, whereas gp12 of T7 was 61.5% identical to KP32 tail protein YP_003347550.1 (100% sequence coverage), locus tag KP32gp32. These high-sequence identities strongly suggest the same portal tail architecture of proteins within these two phages (Fig. 7). Analogous to T7, we proposed that the KP32 portal, attached to its icosahedral capsid shell, was formed by a dodecameric KP32gp31 (YP_003347549.1) and a hexameric KP32gp32 (YP_003347550.1). This portal formed a channel for viral DNA packaging and ejection (Fig. 7A). Being a tailed phage, *Przondovirus* KP32 exploits the KP32gp37-KP32gp38 depolymerase system, which serves to recognize host cell receptors (Fig.7). The portal directly engaged KP32gp37 through interactions with its N-terminal adapter. In turn, KP32gp37 engaged KP32gp38 depolymerase through interactions with its N-terminal hook (Fig. 7, and Supplementary Fig. S2). This branched model allowed the phage KP32 to carry 12 depolymerase molecules on a single virion, 6 of which had K21 and 6 with K3 serotype specificity. In this model, the RBP system pointed toward the capsid, as proposed for the T7 phage [31]. Indeed, it is well-established that communication between the portal, DNA, and the enclosing capsid shell is a normal part of phage biology [49,50].

In conclusion, our results highlight several novel features of the *Przondovirus* KP32 RBP system. Acting as a complex branched molecular machinery, the phage KP32 can efficiently recognize and hydrolyze bacterial CPS. In the case of KP32gp38, K21-type CPS hydrolysis also acts as an immune cell stimulator through the activation of DCs. All of these findings support the use of depolymerases not only to synergize antibiotic treatment but also to produce immunostimulating agents in vaccination strategies against *K. pneumoniae*. By degrading CPS, depolymerases not only increase the permeability of the cell wall and allow access to antibiotics, but they also activate the immune system. Therefore, combined depolymerase-antibiotic therapy may be a solution for the complete eradication of bacterial colonization. In addition, depolymerase products show potential as vaccine antigens. Bacterial polysaccharides are generally conjugated to a carrier protein, like the tetanus toxoid, for a more robust immune response [51]. In our view, the best protective vaccine antigens could be obtained by conjugating K21-pyr5 (and analogs obtained from the depolymerase treatment of other *K. pneumoniae* serotypes) in multiple copies on the surface of conserved protein antigens against *K. pneumoniae*. Structural vaccinology would be of extreme help in the identification of the most proper protein antigens to achieve optimal size for lymphocyte recognition, strong immunogenicity, and cross-protection against the most dangerous serotypes of *K. pneumoniae*. Further in vivo studies are needed to assess the potential of phage depolymerase oligosaccharide products, both alone and in conjugation with protein antigens.

Declarations

Funding: This work was supported by the project INF-ACT “One Health Basic and Translational Research Actions addressing Unmet Needs on Emerging Infectious Diseases” PE00000007, PNRR Mission 4, EU “NextGen-erationEU”- D.D. MUR Prot. no. 0001554 of 11/10/2022, CUP B53C20040570005, by the National Science Centre, Poland (grant UMO-2017/26/M/NZ1/00233) and by the project TENET – “Targeting bacterial cell ENvelope to reverse rEsisTance in emerging pathogens”, 202288EJ8B, funded by Next Generation EU, Mission 4, CUP B53D2301595 0006. F.S. was supported by MUR through the PRIN2020 CANNOT-ESKAPE (2020XNFH9R): Targeting baCteriAl cell eNvelope of Nosocomial paThogens to ESKAPE resistance, 2021–2024.

Declaration of competing interest: None declared.

Ethical approval: Not required.

Data availability: Not applicable.

Supplementary materials

Supplementary material associated with this article can be found, in the online version, at doi:10.1016/j.ijantimicag.2025.107596.

References

[1] Chinemerem Nwobodo D, Ugwu MC, Oliseloke Anie C, Al-Ouqaili MTS, Chinedu Ikem J, Victor Chigozie U, et al. Antibiotic resistance: the challenges and some emerging strategies for tackling a global menace. J Clin Lab Anal 2022;36:e24655. doi:10.1002/jcla.24655.
[2] Naddaf M. 40 million deaths by 2050: toll of drug-resistant infections to rise by 70%. Nature 2024;633:747–8. doi:10.1038/d41586-024-03033-w.
[3] Ho CS, Wong CTH, Aung TT, Lakshminarayanan R, Mehta JS, Rauz S, et al. Ting DSJ. Antimicrobial resistance: a concise update. Lancet Microbe 2025;6(1):100947.
[4] Mulani MS, Kamble EE, Kumkar SN, Tawre MS, Pardesi KR. Emerging strategies to combat ESKAPE pathogens in the era of antimicrobial resistance: a review. Front Microbiol 2019;10:539. doi:10.3389/fmicb.2019.00539.
[5] De Oliveira DMP, Forde BM, Kidd TJ, Harris PNA, Schembri MA, Beatson SA, et al. Antimicrobial resistance in ESKAPE pathogens. Clin Microbiol Rev 2020;33:e00181-19. doi:10.1128/CMR.00181-19.
[6] Dong N, Yang X, Chan EW-C, Zhang R, Chen S. *Klebsiella* species: taxonomy, hypervirulence and multidrug resistance. EBioMedicine 2022;79:103998. doi:10.1016/j.ebiom.2022.103998.
[7] Ashurst JV, Dawson A. *Klebsiella Pneumonia*. StatPearls. Treasure IslandFL: StatPearls Publishing; 2024.
[8] Paczosa MK, Mecsas J. *Klebsiella pneumoniae*: going on the offense with a strong defense. Microbiol Mol Biol Rev 2016;80:629–61. doi:10.1128/MMBR.00078-15.
[9] Bengoechea JA, Sa Pessoa J. *Klebsiella pneumoniae* infection biology: living to counteract host defences. FEMS Microbiol Rev 2019;43:123–44. doi:10.1093/femsre/fuy043.
[10] Opoku-Temeng C, Kobayashi SD, DeLeo FR. *Klebsiella pneumoniae* capsule polysaccharide as a target for therapeutics and vaccines. Comput Struct Biotechnol J 2019;17:1360–6. doi:10.1016/j.csbj.2019.09.011.
[11] Poerio N, Olimpieri T, Henrici De Angelis L, De Santis F, Thaller MC, D'Andrea MM, et al. Fighting MDR-*Klebsiella pneumoniae* infections by a combined host- and pathogen-directed therapeutic approach. Front Immunol 2022;13:835417. doi:10.3389/fimmu.2022.835417.
[12] Anand T, Virmani N, Kumar S, Mohanty AK, Pavulraj S, Bera BC, et al. Phage therapy for treatment of virulent *Klebsiella pneumoniae* infection in a mouse model. J Glob Antimicrob Resist 2020;21:34–41. doi:10.1016/j.jgar.2019.09.018.
[13] Krut O, Bekeredjian-Ding I. Contribution of the immune response to phage therapy. J Immunol 2018;200:3037–44. doi:10.4049/jimmunol.1701745.
[14] Li M, Li P, Chen L, Guo G, Xiao Y, Chen L, et al. Identification of a phage-derived depolymerase specific for KL64 capsule of *Klebsiella pneumoniae* and its anti-biofilm effect. Virus Genes 2021;57:434–42. doi:10.1007/s11262-021-01847-8.
[15] Li P, Guo G, Zheng X, Xu S, Zhou Y, Qin X, et al. Therapeutic efficacy of a K5-specific phage and depolymerase against *Klebsiella pneumoniae* in a mouse model of infection. Vet Res 2024;55:59. doi:10.1186/s13567-024-01311-z.
[16] Maciejewska B, Squeglia F, Latka A, Privitera M, Olejniczak S, Switala P, et al. *Klebsiella* phage KP34gp57 capsular depolymerase structure and function: from a serendipitous finding to the design of active mini-enzymes against K. pneumoniae. mBio 2023;14:e0132923. doi:10.1128/mbio.01329-23.
[17] Squeglia F, Maciejewska B, Łątka A, Ruggiero A, Briers Y, Drulis-Kawa Z, et al. Structural and functional studies of a *Klebsiella* phage capsule depolymerase tailspike: mechanistic insights into capsular degradation. Structure 2020;28:613–24 e4. doi:10.1016/j.str.2020.04.015.
[18] Mirzaie A, Ranjbar R. Antibiotic resistance, virulence-associated genes analysis and molecular typing of *Klebsiella pneumoniae* strains recovered from clinical samples. AMB Express 2021;11:122. doi:10.1186/s13568-021-01282-w.

[19] Masuko T, Minami A, Iwasaki N, Majima T, Nishimura S-I, Lee YC. Carbohydrate analysis by a phenol–sulfuric acid method in microplate format. Analyt Biochem 2005;339:69–72. doi:10.1016/j.ab.2004.12.001.
[20] Minor W, Cymborowski M, Otwinowski Z, Chruszcz M. *HKL* -3000: the integration of data reduction and structure solution – from diffraction images to an initial model in minutes. Acta Crystallogr D Biol Crystallogr 2006;62:859–66. doi:10.1107/S0907444906019949.
[21] Emsley P, Lohkamp B, Scott WG, Cowtan K. Features and development of *Coot*. Acta Crystallogr D Biol Crystallogr 2010;66:486–501. doi:10.1107/S0907444910007493.
[22] Winn MD, Ballard CC, Cowtan KD, Dodson EJ, Emsley P, Evans PR, et al. Overview of the CCP4 suite and current developments. Acta Crystallogr D Biol Crystallogr 2011;67:235–42. doi:10.1107/S0907444910045749.
[23] Abramson J, Adler J, Dunger J, Evans R, Green T, Pritzel A, et al. Accurate structure prediction of biomolecular interactions with AlphaFold 3. Nature 2024;630:493–500. doi:10.1038/s41586-024-07487-w.
[24] Chen H, Schürch CM, Noble K, Kim K, Krutzik PO, O'Donnell E, et al. Functional comparison of PBMCs isolated by cell preparation tubes (CPT) vs. lymphoprep tubes. BMC Immunol 2020;21:15. doi:10.1186/s12865-020-00345-0.
[25] Fallarini S, Cerofolini L, Salobehaj M, Rizzo D, Gheorghita GR, Licciardi G, et al. Site-selective functionalized PD-1 mutant for a modular immunological activity against cancer cells. Biomacromolecules 2023;24:5428–37. doi:10.1021/acs.biomac.3c00893.
[26] Dutton GGS, Choy YM. Capsular polysaccharide from *Klebsiella* type 21. Carbohydr Res 1972;21:169–72. doi:10.1016/S0008-6215(00)81745-0.
[27] Krissinel E, Henrick K. Inference of macromolecular assemblies from crystalline state. J Mol Biol 2007;372:774–97. doi:10.1016/j.jmb.2007.05.022.
[28] Laskowski RA, Swindells MB. LigPlot+: multiple ligand–protein interaction diagrams for drug discovery. J Chem Inf Model 2011;51:2778–86. doi:10.1021/ci200227u.
[29] Latka A, Leiman PG, Drulis-Kawa Z, Briers Y. Modeling the architecture of depolymerase-containing receptor binding proteins in *Klebsiella* phages. Front Microbiol 2019;10:2649. doi:10.3389/fmicb.2019.02649.
[30] Abramson J, Adler J, Dunger J, Evans R, Green T, Pritzel A, et al. Accurate structure prediction of biomolecular interactions with AlphaFold 3. Nature 2024;630:493–500. doi:10.1038/s41586-024-07487-w.
[31] Chen W, Xiao H, Wang L, Wang X, Tan Z, Han Z, et al. Structural changes in bacteriophage T7 upon receptor-induced genome ejection. Proc Natl Acad Sci USA 2021;118:e2102003118. doi:10.1073/pnas.2102003118.
[32] Garcia-Doval C, Castón J, Luque D, Granell M, Otero J, Llamas-Saiz A, et al. Structure of the receptor-binding carboxy-terminal domain of the bacteriophage T5 L-shaped tail fibre with and without its intra-molecular chaperone. Viruses 2015;7:6424–40. doi:10.3390/v7122946.
[33] Schwarzer D, Stummeyer K, Gerardy-Schahn R, Mühlenhoff M. Characterization of a novel intramolecular chaperone domain conserved in endosialidases and other bacteriophage tail spike and fiber proteins. J Biol Chem 2007;282:2821–31. doi:10.1074/jbc.M609543200.
[34] Xiang Y, Leiman PG, Li L, Grimes S, Anderson DL, Rossmann MG. Crystallographic insights into the autocatalytic assembly mechanism of a bacteriophage tail spike. Mol Cell 2009;34:375–86. doi:10.1016/j.molcel.2009.04.009.
[35] Karampatakis T, Tsergouli K, Behzadi P. Carbapenem-resistant *Klebsiella pneumoniae*: virulence factors, molecular epidemiology and latest updates in treatment options. Antibiotics (Basel) 2023;12:234. doi:10.3390/antibiotics12020234.
[36] Opoku-Temeng C, Kobayashi SD, DeLeo FR. *Klebsiella pneumoniae* capsule polysaccharide as a target for therapeutics and vaccines. Comput Struct Biotechnol J 2019;17:1360–6. doi:10.1016/j.csbj.2019.09.011.
[37] Tu I-F, Lin T-L, Yang F-L, Lee I-M, Tu W-L, Liao J-H, et al. Structural and biological insights into *Klebsiella pneumoniae* surface polysaccharide degradation by a bacteriophage K1 lyase: implications for clinical use. J Biomed Sci 2022;29:9. doi:10.1186/s12929-022-00792-4.
[38] Huang T, Zhang Z, Tao X, Shi X, Lin P, Liao D, et al. Structural and functional basis of bacteriophage K64-ORF41 depolymerase for capsular polysaccharide degradation of *Klebsiella pneumoniae* K64. Int J Biol Macromol 2024;265:130917. doi:10.1016/j.ijbiomac.2024.130917.
[39] Dunstan RA, Bamert RS, Belousoff MJ, Short FL, Barlow CK, Pickard DJ, et al. Mechanistic insights into the capsule-targeting depolymerase from a *Klebsiella pneumoniae* bacteriophage. Microbiol Spectr 2021;9:e0102321. doi:10.1128/Spectrum.01023-21.
[40] Cai R, Ren Z, Zhao R, Lu Y, Wang X, Guo Z, et al. Structural biology and functional features of phage-derived depolymerase Depo32 on *Klebsiella pneumoniae* with K2 serotype capsular polysaccharides. Microbiol Spectr 2023;11:e05304-22. doi:10.1128/spectrum.05304-22.
[41] Hsieh P-F, Lin H-H, Lin T-L, Chen Y-Y, Wang J-T. Two T7-like bacteriophages, K5-2 and K5-4, each encodes two capsule depolymerases: isolation and functional characterization. Sci Rep 2017;7:4624. doi:10.1038/s41598-017-04644-2.
[42] Majkowska-Skrobek G, Latka A, Berisio R, Squeglia F, Maciejewska B, Briers Y, et al. Phage-borne depolymerases decrease *Klebsiella pneumoniae* resistance to innate defense mechanisms. Front Microbiol 2018;9:2517. doi:10.3389/fmicb.2018.02517.
[43] Danner M, Fuchs A, Miller S, Seckler R. Folding and assembly of phage P22 tailspike endorhamnosidase lacking the N-terminal, head-binding domain. Eur J Biochem 1993;215:653–61. doi:10.1111/j.1432-1033.1993.tb18076.x.
[44] Garcia-Doval C, Van Raaij MJ. Crystallization of the C-terminal domain of the bacteriophage T7 fibre protein gp17. Acta Crystallogr F Struct Biol Cryst Commun 2012;68:166–71. doi:10.1107/S1744309111051049.
[45] Galan Bartual S, Garcia-Doval C, Alonso J, Schoehn G, Van Raaij MJ. Two-chaperone assisted soluble expression and purification of the bacteriophage T4 long tail fibre protein gp37. Prot Expr Purif 2010;70:116–21. doi:10.1016/j.pep.2009.11.005.
[46] Granell M, Namura M, Alvira S, Garcia-Doval C, Singh AK, Gutsche I, et al. Crystallization of the carboxy-terminal region of the bacteriophage T4 proximal long tail fibre protein gp34. Acta Crystallogr F Struct Biol Commun 2014;70:970–5. doi:10.1107/S2053230X14010449.
[47] Matsui T, Griniuviené B, Goldberg E, Tsugita A, Tanaka N, Arisaka F. Isolation and characterization of a molecular chaperone, gp57A, of bacteriophage T4. J Bacteriol 1997;179:1846–51. doi:10.1128/jb.179.6.1846-1851.1997.
[48] Raaij MJV, Schoehn G, Jaquinod M, Ashman K, Burda MR, Miller S. Identification and crystallisation of a heat- and protease-stable fragment of the bacteriophage T4 short tail fibre. Biol Chem 2001;382. doi:10.1515/BC.2001.131.
[49] Lokareddy RK, Sankhala RS, Roy A, Afonine PV, Motwani T, Teschke CM, et al. Portal protein functions akin to a DNA-sensor that couples genome-packaging to icosahedral capsid maturation. Nat Commun 2017;8:14310. doi:10.1038/ncomms14310.
[50] Maurer JB, Oh B, Moyer CL, Duda RL. Capsids and portals influence each other's conformation during assembly and maturation. J Mol Biol 2020;432:2015–29. doi:10.1016/j.jmb.2020.01.022.
[51] Bloom DE, Black S, Salisbury D, Rappuoli R. Antimicrobial resistance and the role of vaccines. Proc Natl Acad Sci USA 2018;115:12868–71. doi:10.1073/pnas.1717157115.